Seawater temperature and salinity sensing based on in-fiber Michelson-Fabry-Perrot hybrid interferometer employing frequency domain decomposition method*

WANG Jiahui[1], WEI Xian[2], ZHU Yan[2], SHEN Yue[2], PANG Lipeng[3], and DUAN Shaoxiang[1,4]**

1. Institute of Modern Optics, Tianjin Key Laboratory of Micro-scale Optical Information Science and Technology, Nankai University, Tianjin 300350, China

2. Foreign Cooperation Projects Department of PetroChina Dagang Oilfield Company, Tianjin 300280, China

3. The 58th Research Institute of China Electronics Technology Group Corporation, Wuxi 214035, China

4. Southern Marine Science and Engineering Guangdong Laboratory, Zhuhai 519000, China

(Received 14 April 2023; Revised 20 July 2023)

We propose an in-fiber Michelson-Fabry-Perrot (M-FP) hybrid interferometer for the simultaneous measurement of seawater temperature and salinity. The sensor head consists of two parallel hetero Fabry-Perot (FP) cavities fabricated on the end face of the twin core fiber (TCF). A fiber fusion taper is used to split and recouple the light in the two cores. In this case, the Vernier effect can be obtained which can greatly enhance the sensitivity and solve the problem of temperature cross-sensitivity. Different from the traditional demodulation method based on envelop detection, we employed frequency domain decomposition method (FDDM) to demodulate the sensing signal. The simulation results indicate that the proposed sensor has high sensitivity to salinity and temperature. Thanks to the merits of high sensitivity, ease of fabrication and small footprint, the proposed seawater temperature and salinity sensor would have potential applications in marine science, food industry and ocean ranching.

Document code: A **Article ID:** 1673-1905(2024)02-0070-6

DOI https://doi.org/10.1007/s11801-024-3070-0

Seawater salinity is a parameter that measures the number of dissolved substances contained in seawater[1]. It is a key parameter in our study of ocean hydrology. Seawater salinity sensors have been widely used in seabed biological resources search, marine mineral resources and clean energy exploitation. The existing salinity sensors are mainly electrical sensors[2] as well as optical sensors. Compared with electrical sensors, optical sensors have the advantages of higher sensitivity, easy integration and networking, and long-term online real-time monitoring[3]. Among the optical salinity sensors, optical fiber salinity sensors have received wide attention because of their compact structure and high sensitivity. The mechanism of the fiber optic salinity sensors can be divided into two categories: sensing materials coating[4,5] and refractive index (RI) measurements[6-8].

As one of the key sensing schemes, the RI-based salinity Fabry-Perot (FP) fiber sensors would be more attractive, due to advantages of fast response time, high sensitivity and good reproductively. In 2022, LI et al[9] proposed a reflective fiber-optic FP salinity sensor based on two sections of single mode fiber (SMF) and achieve a sensitivity of 2.508 83 nm/‰. After that, WANG et al[10] proposed a high-resolution salinity sensor with salinity resolution as low as 0.005 8‰ based on a self-referenced parallel FP fiber microcavity. In 2021, NIU et al[11] designed a composite dual-cavity fiber FP salinity sensor based on hollow core fiber. By employing the intensity modulation, the sensitivity can be 0.101/%, i.e., 0.010 1/part per thousand (ppt). Although these schemes have highly improved the performance of the salinity sensors, the new salinity sensing schemes with higher sensitivity and capability of addressing cross-sensitivity are still worthy of further study.

In this letter, an in-fiber Michelson-Fabry-Perrot (M-FP) hybrid interferometer is proposed for the simultaneous measurement of seawater temperature and salinity. We firstly analyzed the influence of salinity and temperature to the seawater RI, and discussed the mechanism of temperature and salinity sensing based on RI measurement. Then, we designed an in-line M-FP interferometer to enhance the light interaction with seawater and utilize the Vernier effect to improve the performance and achieve the simultaneous measurement of

* This work has been supported by the National Natural Science Foundation of China (Nos.62275131, 62231005 and 62105164), and the Natural Science Foundation of Tianjin (Nos.21JCQNJC00210, 22JCQNJC01540 and 21JCYBJC00080).

** E-mail: sxduan@nankai.edu.cn

temperature and salinity. Moreover, the refractive-temperature cross-sensitivity was compensated by solving a sensitivity-coefficient matrix equation for the two FP cavities. The proposed sensor possesses the advantages of high sensitivity, small size as well as ease of fabrication, and can be applied in many fields such as marine science, food industry and ocean ranching.

In order to reveal the sensing mechanism of the RI based salinity sensors, we firstly analyze the seawater RI model. The empirical model of salinity RI of seawater applicable to optical sensing is proposed by QUAN et al[12] and shown as follows

$$n(S,T,\lambda)=n_0+(n_1+n_2T+n_3T^2)S+n_4T^2+\frac{(n_5+n_6S+n_7T)}{\lambda}+\frac{n_8}{\lambda^2}+\frac{n_9}{\lambda^3}, \quad (1)$$

where S and T represent the salinity and temperature, respectively, λ is wavelength, n_1—n_9 are constants, and their values are 1.314 105, 1.779×10^{-4}, -1.05×10^{-6}, 1.6×10^{-8}, -2.02×10^{-6}, 15.868, 0.011 55, −0.042 3, −4 382, $1.145\ 5\times10^{6}$. According to this equation formula, we can see that the seawater RI is mainly affected by temperature, salinity and wavelength of incident light. We mapped the RI at different temperatures and salinities, when the wavelength of incident light is 600 nm, as shown in Fig.1. The temperature range is from 0 to 30 °C, and the salinity range is from 0 to 35 ppt. Fig.1 indicates that the seawater RI increases gradually with the increase of salinity, but shows the opposite property with the increase of temperature. To clearly see all the impact factors to the seawater RI including wavelength, we calculate the RI difference when the wavelength increases from 550 nm to 551 nm, as shown in Fig.2.

We can observe that the seawater RI varies from -4.98×10^{-5} to -4.78×10^{-5} when the wavelength is changed by 1 nm at constant temperature and salinity, which shows that the RI of seawater decreases as the wavelength of incident light increases. What calls for special attention is that the amount of change is not obvious but not negligible.

According to the analysis above, it is clear that the RI of seawater has a certain variation relationship with salinity. Therefore, the salinity of seawater can be characterized indirectly by measuring the RI of seawater. Furthermore, the salinity sensor based on this mechanism should address the problem of temperature cross-sensitivity at the same time of salinity measurement.

To address the temperature cross-sensitivity, we employ a hybrid interferometer cascaded with an in-fiber Michelson interferometer and two parallel FP cavities, and then utilize the sensitivity difference to temperature and salinity to establish the demodulation matrix. The structure configuration of the interferometer is shown in Fig.3. A twin core fiber (TCF) is connected with a section of SMF by a polymer microfiber. It should be noticed that the polymer fiber should cover one of the fiber

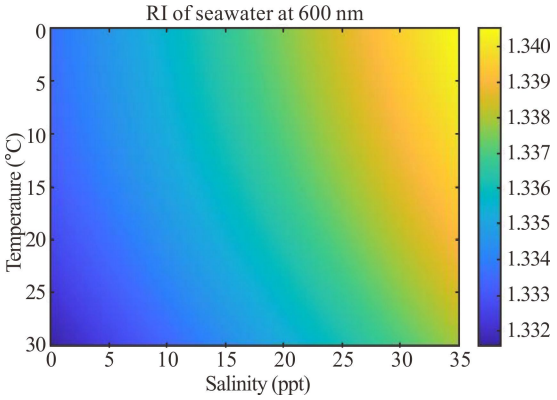

Fig.1 RI of seawater versus temperature and salinity when the wavelength of incident light is 600 nm

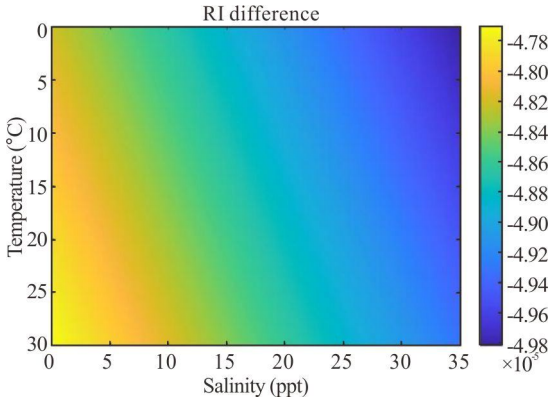

Fig.2 RI difference versus temperature and salinity with wavelength variation of 1 nm

cores of TCF, so that parallel hetero FP cavities can be achieved. The open FP cavity is to enhance the light interaction with the seawater. The optical path of the hybrid interferometer is also provided in Fig.3. Simultaneously, the optical path difference of the sensor can be dynamically modulated through alterations in the material properties of the polymer fiber. The reflectivity of each end face of open cavity is r_1 and r_2, respectively, and r_3 and r_4 for the solid cavity, respectively. The values of the reflectivity can be calculated by the well-known Fresnel formula. Then, the reflection intensities of each core can be expressed as

$$E_{oa}=E_{ia}r_1+E_{ia}(1-r_1r_1^*)r_2\exp(-i\varphi_1), \quad (2)$$

$$E_{ob}=E_{ib}r_3+E_{ib}(1-r_3r_3^*)r_4\exp(-i\varphi_2), \quad (3)$$

where E_{ia} and E_{ib} are the amplitudes of light field separated from the input light by the fusion tapered slicing. E_{oa} and E_{ob} are the amplitudes of light field reflected by the parallel FP cavities. $\varphi_1=4\pi n_1L/\lambda$ and $\varphi_2=4\pi n_2L/\lambda$ are the phases of the light reflected by the second facet through the cavities. n_1 and n_2 are the RIs of seawater and polymer fiber, respectively. n_1 is determined by Eq.(1) and n_2=1.405. L is the length of the cavity. When the reflected light beams are coupled back to the SMF, the electric field of the output light can be expressed as

$$E_o=E_{oa}\exp(i\varphi_0)+E_{ob}\exp(i\varphi_0), \quad (4)$$

where φ_0 is the phase variation when the light propagates

through the TCF. Then, the intensity of the output light can be expressed as

$$I_o = E_o E_o^*. \quad (5)$$

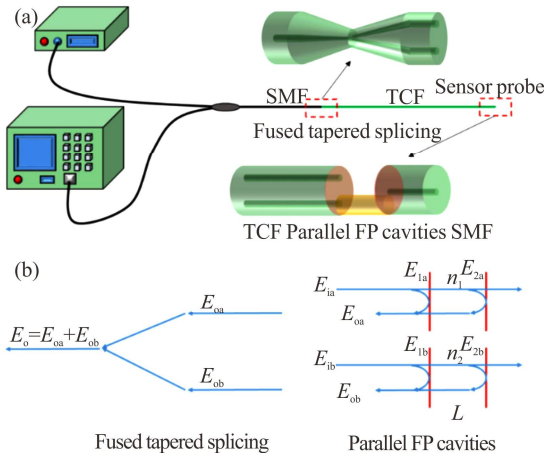

Fig.3 Microfiber-assisted cascaded FP interferometer: (a) Structure configuration; (b) Optical path of the hybrid interferometer

According to Eq.(5), the reflection spectrum of the hybrid interferometer is calculated as shown in Fig.4 when L=25 μm. It should be noticed that we considered the material dispersion in numeral analysis by introducing the Selmeyer equation, to precisely calculate the spectrum of the M-FP hybrid interference. As shown in Fig.4, we can observe that there is an envelope that exists at the base interference spectrum, which is a typical spectrum of Vernier effect. We can choose one of the dips and the node of the envelope to demodulate the sensing signal via such spectrum. However, influenced by the interference fringe, the position of the node is hard to precisely obtain.

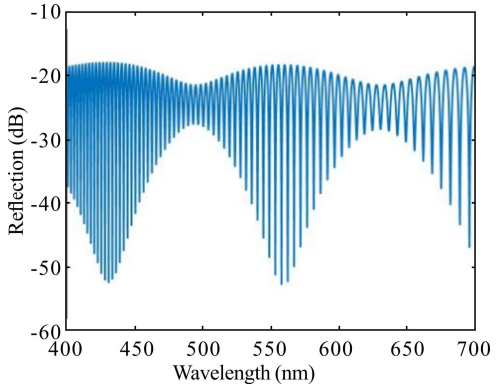

Fig.4 Calculated spectrum of the cascaded FP interferometer when L=25 μm, T=0 °C, and S=15 ppt

To address this problem, we proposed a frequency domain decomposition method (FDDM) to separate out each frequency component. We firstly calculate the Fourier transform (FT) spectrum of interference fringe, as shown in Fig.5. Subsequently, the discrete frequency components are extracted using a band-pass filter, facilitating the segregation and analysis of distinct frequency elements. The FDDM enables the concurrent analysis of multiple mode interference processes while establishing a direct correlation between the fiber interference structure and the resultant output spectrum. It is easy to find that the reflection spectrum contains four frequency components. However, according to Eqs.(2)—(5), there should be three frequency components which are corresponding to the phases φ_1, φ_2 and their difference $\varphi_1-\varphi_2$. The reason for the difference between the FT results and the theoretical analysis is the existence of the material dispersion. For another aspect, as the phase is inversely proportional to λ, i.e., the wavelength of the light source, the interference fringes exhibit chirp line-shape, which is dense in short wavelength but sparse in long wavelength. As a result, the characteristic frequencies of the interference in FT spectrum will be broadened. When the two adjacent frequency bands overlapped, new frequency peak will be generated in the FT spectrum.

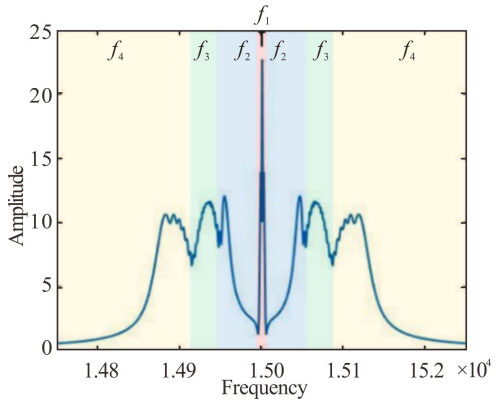

Fig.5 Fourier transform of the reflection spectrum, f_1, f_2, f_3 and f_4 are corresponding to the pass bands of the filters, respectively

We extract the interference fringes with each frequency by filtering out the other frequency components, as shown in Fig.6. We can clearly observe the interference fringe with different frequencies. However, due to the influence of the material dispersion, the passed frequencies have a certain bandwidth during the filter processing, which makes the fringes not exhibit regular sinusoidal line shape. Despite all this, we can also easily obtain different sensing properties by FDDM, which can be used to solve the cross-sensitivity.

Since the RI of seawater is simultaneously affected by the salinity and temperature, here, we model and analyze the sensing characteristics of salinity and temperature, respectively and solve the cross-sensitivity problem by establishing a demodulation matrix. Because the salinity of the seawater near the coast of China varies in the range from 15 ppt to 35 ppt and the temperature changes from 0 to 30 °C, we set this salinity and temperature ranges as the measurement ranges in our discussion.

We firstly discuss the salinity sensing performance. Note that the simulation keeps the geometric parameters of the M-FP hybrid interferometer unchanged and the temperature at T=0 °C. We gradually increase the salinity from 15 ppt to 35 ppt and then calculated the spectra

according to Eqs.(2)—(5), as shown in Fig.7. To describe the response characteristics more intuitively, each salinity gradient was introduced with a 20 dB offset. We can observe that the nodes of the interference fringes gradually move towards the short wavelength. By using the FDDM, we obtain four spectral components corresponding to the characteristic frequency bands of f_1, f_2, f_3 and f_4, respectively, as shown in Fig.8.

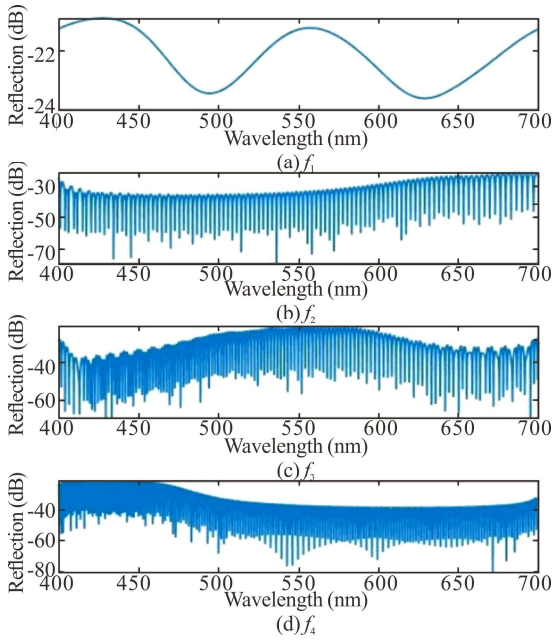

Fig.6 Reflection spectra with different frequency components (respectively for f_1, f_2, f_3 and f_4 from top to bottom)

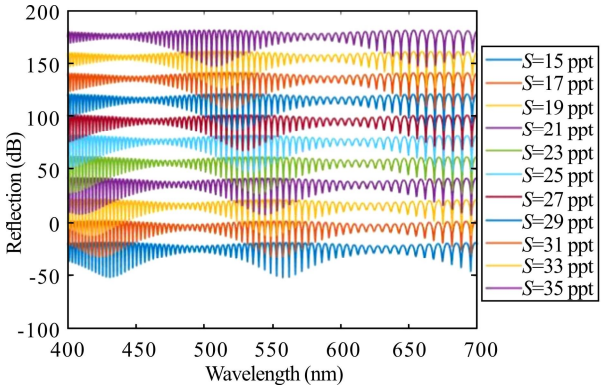

Fig.7 Reflection spectra under different salinities

We choose a dip around 490 nm in each component to analyze the sensing response. For component 1, the dip varies linearly from 493.92 nm to 436.09 nm with the increasing of the salinity. The sensitivity can be up to −2.989 86 nm/ppt. Unlike component 1, the dips of the other components shift to the long wavelength with the increasing of salinity, as shown in the inset in Fig.9. The shifts of the dips are all about 2 nm. The sensitivities are 0.132 05 nm/ppt, 0.073 05 nm/ppt and 0.100 91 nm/ppt, respectively. The sensing responses are listed in Tab.1. We can clearly see that the sensitivity of low frequency component is much higher than the other components, which demonstrates that the Vernier effect can dramatically enhance the sensitivity of the sensors.

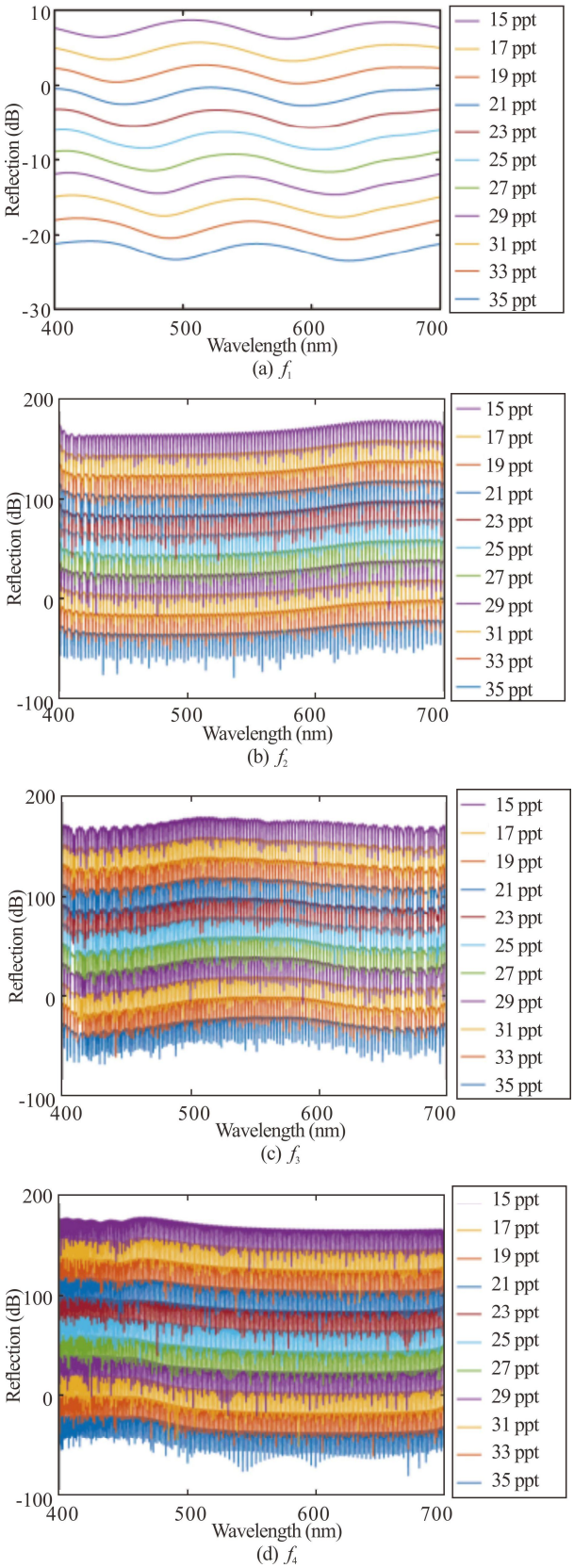

Fig.8 Reflectance spectral components under different salinities

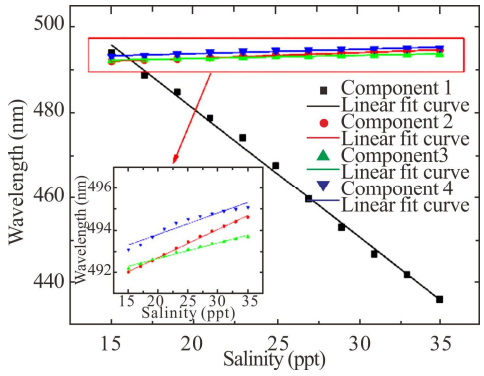

Fig.9 Salinity sensing responses of the four components

Tab.1 Salinity sensing responses for the for components

	Sensitivity (nm/ppt)	*R*-square
Component 1	−2.989 86	0.995 28
Component 2	0.132 05	0.996 37
Component 3	0.073 05	0.983 09
Component 4	0.100 91	0.929 85

Then, we keep the salinity at S=15 ppt and gradually increase the temperature T with a step of 3 ℃. The calculated spectra under different temperatures are shown in Fig.10. We also use the FDDM to separate out the four components, as shown in Fig.11. We track the selected dips of the four components as the increasing of temperature. The sensing response can be observed in Fig.12. According to Fig.1, the influence of temperature to the RI of seawater is opposite to that of salinity. Then, the temperature sensing responses of high frequency components should be opposite to the salinity. However, Fig.12 indicates that the temperature sensing properties of high frequency components are similar to those of salinity. The reason is that we consider the thermo-expansion of the FP cavities in analysis. Because the influence of the thermo-expansion effect to the phase variation is higher than thermo-optical effect, the dips move towards the long wavelength. Because component 1 corresponds to the phase difference $\varphi_1-\varphi_2$, the effect of thermo-expansion can be canceled out. Thus, the component 1 shows the opposite behavior to the salinity, which is different from other components. To clearly see the temperature sensing response of the proposed sensor, we also summary the sensitivities and linearity in Tab.2.

In order to solve the cross-sensitivity problem, we can select two components and establish a demodulation matrix. Considering the linearity of the response curve, we choose component 1 and component 3. Then, the sensing signal can be demodulated by the following expression

$$\begin{pmatrix}\Delta S\\ \Delta T\end{pmatrix}=\begin{pmatrix}-2.989\,86\ \text{nm/ppt} & 4.512\,64\ \text{nm/°C}\\ 0.073\,05\ \text{nm/ppt} & 0.082\,52\ \text{nm/°C}\end{pmatrix}^{-1}\begin{pmatrix}\Delta\lambda_1\\ \Delta\lambda_3\end{pmatrix}, \quad (6)$$

where $\Delta\lambda_1$ and $\Delta\lambda_3$ correspond to the wavelength variations of the dips of component 1 and component 3, respectively. ΔS is the variation of salinity and ΔT is the variation of temperature. Then, we can achieve the simultaneous measurement of salinity and temperature with high sensitivity.

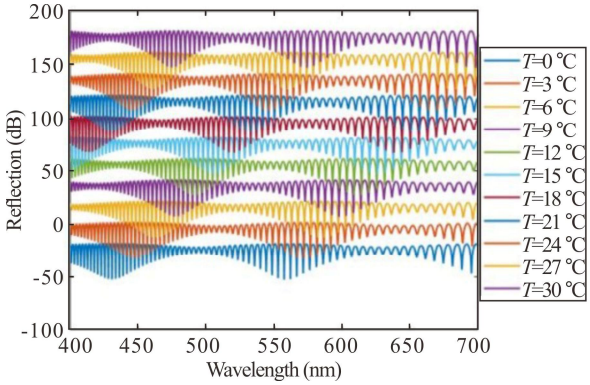

Fig.10 Reflection spectra under different temperatures

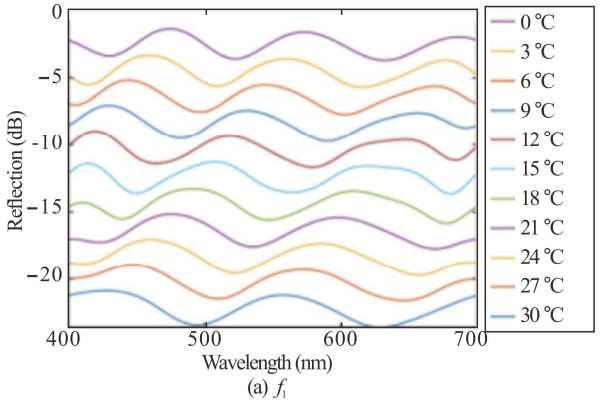

(a) f_1

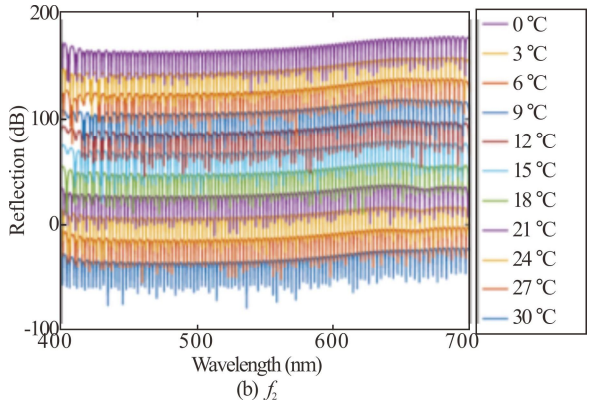

(b) f_2

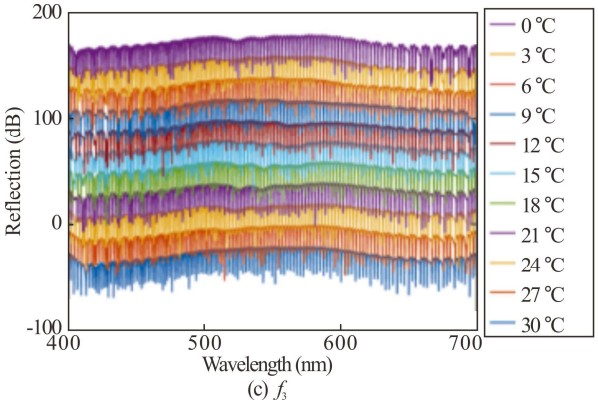

(c) f_3

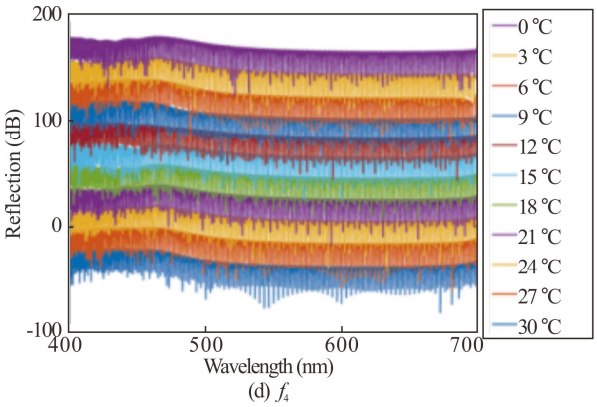

Fig.11 Reflectance spectral components under different temperatures

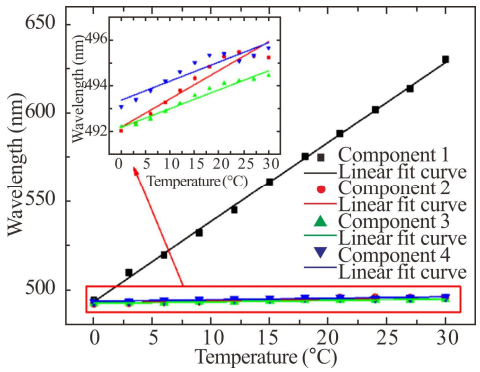

Fig.12 Temperature sensing responses of the four components

Tab.2 Temperature sensing responses for the four components

	Sensitivity (nm/°C)	*R*-square
Component 1	4.512 64	0.998 58
Component 2	0.124 48	0.918 79
Component 3	0.082 52	0.967 52
Component 4	0.083 85	0.875 60

In this work, we proposed an in-fiber M-FP hybrid interferometer for simultaneous measurement of seawater temperature and salinity. By introducing multiple interferometric structures, the Vernier effect can be obtained, which can greatly enhance the sensitivity and solve the problem of cross-sensitivity. We proposed an FDDM to analyze the sensing performance of different characteristic frequency components and demodulate the sensing signal. The simulation results indicate that the proposed sensor has high sensitivities to salinity and temperature. Due to the advantages of high sensitivity, ease of fabrication and small footprint, the proposed sensor would have potential applications in marine science, food industry and ocean ranching.

Ethics declarations

Conflicts of interest

The authors declare no conflict of interest.

References

[1] WOOSLEY R J, HUANG F, MILLERO F J. Estimating absolute salinity (SA) in the world's oceans using density and composition[J]. Deep sea research part I: oceanographic research papers, 2014, 93: 14-20.

[2] XU M X, ZHANG X N, CHAI X, et al. Design of marine salinity sensor based on boron-doped diamond film electrode[J]. Journal of ocean technology, 2022, 41(02): 12-19.

[3] SHEN L, JIANG J F, WANG S, et al. Fiber laser salinity sensing based on micro-tubule[J]. Journal of optoelectronics·laser, 2022, 33(01): 1-8. (in Chinese)

[4] WANG H, LIANG C, BAO X. Salinity concentration sensing based on a tapered dual-core as As_2Se_3-PMMA hybrid fiber[J]. IEEE photonics technology letters, 2021, 33(4): 181-184.

[5] SAMAVATI Z, SAMAVATI A, ISMAIL A, et al. Role of outer layer configuration on saline concentration sensitivity of optical fiber probe coated with ZnO/Ag nano-heterostructure[J]. Optics & laser technology, 2021, 136: 106722.

[6] ZHAO Y, ZHAO J, WANG X, et al. Femtosecond laser-inscribed fiber-optic sensor for seawater salinity and temperature measurements[J]. Sensors and actuators B: chemical, 2022, 353: 131134.

[7] ZHAO J, ZHAO Y, CAI L. Hybrid fiber-optic sensor for seawater temperature and salinity simultaneous measurements[J]. Journal of lightwave technology, 2022, 40(3): 880-886.

[8] WANG Y, TONG R, ZHAO K, et al. Optical fiber sensor based on SPR and MZI for seawater salinity and temperature measurement[J]. Optics & laser technology, 2023, 162: 109315.

[9] LI Z, LI L, ZHANG Y, et al. Highly-sensitive fiber-optic FP salinity sensor based on Vernier effect[J]. Optical fiber technology, 2022, 74: 103148.

[10] WANG L, GENG Y, LI X, et al. High-resolution optical fiber salinity sensor with self-referenced parallel Fabry-Perot fiber microcavity[J]. IEEE sensors journal, 2022, 23(1): 337-343.

[11] NIU H L, WANG W, SHEN J X, et al. Composite double-cavity fiber Fabry-Perot salinity sensor based on hollow core fiber[J]. Optical instruments, 2021, 43(3): 72-77.

[12] QUAN X, FRY E S. Empirical equation for the index of re-fraction of seawater[J]. Applied optics, 1995, 34(18): 3477-3480.